

Indentation of a pore-spanning lipid bilayer membrane by an AFM tip

Davood Norouzi

Institute for Advanced Studies in Basic Sciences, P.O.Box: 45195-1159, Zanjan, Iran

Martin Michael Müller and Markus Deserno

Max-Planck-Institut für Polymerforschung, Ackermannweg 10, 55128 Mainz, Germany

(Dated: December 2, 2024)

Measurements with an atomic force microscope (AFM) offer a direct way to probe elastic properties of lipid bilayer membranes locally: by poking a pore-spanning membrane with an AFM tip one can determine force-indentation curves. These curves can be described with a generic elasticity model by calculating the exact membrane shapes within the Helfrich theory. Introducing an additional adhesion between tip and membrane via an adhesion balance leads to a more complicated behavior such as a hysteresis in the force-indentation curves. Even if the tip is pulled upwards stable membrane profiles can be found in that case. The maximum pulling force that can be applied before the tip detaches from the membrane depends on the scaled value of adhesion and can be predicted within this model.

PACS numbers: 87.16.Dg, 68.37.Ps, 02.30.Hq

I. INTRODUCTION

Material properties of lipid bilayer membranes are highly important for the functioning of biological cells [1]. In the past, different methods have been applied to determine the values of elastic constants globally in a large variety of setups. Classical instruments for these kinds of studies are optical tweezers [2], micropipettes [3, 4], and atomic force microscopes (AFM) [5, 6].

Global measurements are, however, not sufficient if one is interested in membranes that change their properties on a small scale, *e.g.* due to their composition. Fortunately, the AFM offers a possibility to *locally* measure elastic properties in a well-defined setup: in a recent experiment [7] a pore-spanning lipid bilayer was probed with an AFM tip yielding force-indentation curves. In this paper we want to give the theoretical background necessary to interpret the experimental results under a variety of setup conditions and give motivation for further studies on this subject.

In the following the membrane will be modelled as a two-dimensional fluid with energy contributions stemming from surface tension and bending. In this model the exact shape of the membrane can be determined numerically resulting in force-indentation curves that can be compared with the ones obtained in the experiment [7]. Calculations using similar techniques were done before in studies of vesicle shapes and virus budding [8, 9, 10, 11, 12, 13, 14, 15]. Other investigations close to our approach were made in the context of membrane tube formation [16, 17, 18]: Refs. [16] considered a point force pulling out a tube (“tether”) of a flat membrane. They show that the force needed to move the point away from the membrane increases first to a maximum. Then, it decreases slightly until a force plateau is reached. In Ref. [17] a point force was applied to a membrane vesicle adhering to a flat substrate. There, the competition between tether formation and adhesion of the vesicle to

the substrate was investigated.

In the present work we want to model the force-exerting AFM tip as a spatially extended object rather than a point. We also want to include a possible adhesion energy between the curved tip and the membrane. The area where tip and membrane are in contact is determined by a force balance [19, 20] in contrast to the existing calculations.

Due to the adhesion it is possible to pull the tip upwards and still obtain stable membrane shapes. The force necessary to release the tip from the membrane can be determined as a function of the adhesion strength analogous to Ref. [21] where the unbinding of a cylindrical bead from a membrane was examined.

The paper is structured as follows: in Chapter II we will introduce the model of our system and discuss the relevant energies. In the following Chapter III we present the equations that have to be solved in order to find membrane profiles, force-indentation curves and detachment forces. The results of our calculations are summarized in Chapter IV. The publication ends with Chapter V on a discussion how the predictions for indentation and adhesion characteristics can be used to extract material properties in future experiments.

II. THE MODEL

A. Geometry of the system

We consider a flat solid substrate with a circular pore of radius R_{pore} . A lipid bilayer membrane rests on the substrate and spans the pore. In the situation we want to analyze an AFM tip is used to probe the properties of the free pore-spanning membrane. We assume that the tip has a parabolical shape with curvature radius R_{tip} at its apex. Furthermore, we restrict ourselves to the static axisymmetric situation in which the tip pokes the free-

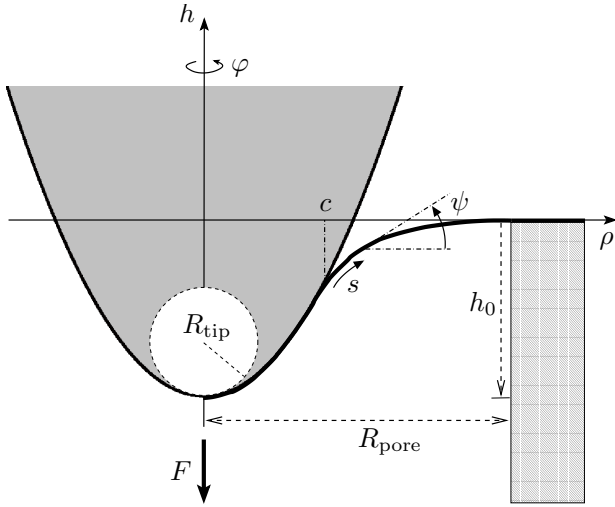


FIG. 1: Illustration of the geometry. A parabolic tip with curvature radius R_{tip} indents a pore-spanning membrane with a force F to a certain extent h_0 . The radius of the pore is R_{pore} . The membrane leaves the tip at the point of detachment $\rho = c$. The two possible parametrizations $h(\rho)$ and $\psi(s)$ are explained in the beginning of Chapter III.

standing membrane exactly in the middle of the pore (see Fig. 1). For a certain downward force $F > 0$ the membrane is indented to a corresponding depth $h_0 > 0$ which is measured from the plane of the substrate to the depth of the apex of the tip. Note that it is also possible to pull out the membrane with a force in the opposite direction if attractive interactions attach the membrane to the tip.

In the following, we will model the bilayer as a two-dimensional surface. This is a valid approach provided the thickness of the membrane (approx. 5 nm) is much smaller than (i) the membrane's lateral extension as well as (ii) length scales of interest such as local radii of curvature.

With these geometric assumptions in mind, let us now consider the different energy contributions we want to include in our model.

B. Energy considerations

The total energy of the system “pore-tip” is made up of several different contributions: the membrane is under a *lateral tension* σ . To pull excess area into the pore, work has to be provided to overcome the adhesion between membrane and flat substrate [22]. It is given by σ times the excess area [23]. Additionally, a *curvature energy* can be associated with the membrane. According to Canham and Helfrich [24, 25] the Hamiltonian for a symmetric membrane is then

$$E_{\text{elast}} = \int_{\Sigma} dA \left(\sigma + \frac{\kappa}{2} K^2 + \bar{\kappa} K_G \right), \quad (1)$$

where Σ denotes the surface of the membrane part which spans the pore. The proportionality constants κ and $\bar{\kappa}$ are called bending rigidity and saddle-splay modulus, respectively. The Gaussian curvature K_G is the product of the two principal curvatures whereas K is their sum [26, 27]. Note that the last term of energy (1) yields zero in our specific problem [28].

With the help of the two material constants σ and κ one can define a characteristic lengthscale

$$\lambda := \sqrt{\frac{\kappa}{\sigma}}, \quad (2)$$

which does not depend on geometric boundary conditions such as the radius of the tip or the pore but only on properties of the membrane. The larger λ is, the more important bending becomes compared to tension.

Apart from tension and bending an *adhesion between tip and membrane* may contribute to the total energy. We assume that it is proportional to the contact area A_{contact} between tip and membrane with a proportionality constant w , the adhesion energy per area.

If the indentation h_0 is given and one wants to determine the force F , the total energy can thus be written as

$$E_{\text{total}}^{h_0} = \int_{\Sigma} dA \left(\sigma + \frac{\kappa}{2} K^2 \right) - w A_{\text{contact}}. \quad (3)$$

Under certain circumstances, however, it is more convenient to consider the problem for a given force F . Both ensembles (“constant indentation” vs. “constant force” ensemble) are connected via a Legendre transformation [13], $E_{\text{total}}^{h_0} = E_{\text{total}}^F - F h_0$, where $F > 0$ is equivalent to indentation.

Note that the ground states one obtains for the two ensembles will be the same whereas questions of stability depend on the ensemble: a profile found to be stable under constant height conditions is not necessarily stable under constant force conditions.

The route we want to follow here in order to find force-indentation curves is to determine the equilibrium shapes of the non-bound section of the membrane via a functional minimization. The energy contributions caused by the bounded section of the membrane enter via the appropriate boundary conditions (see Chapter III and Appendix A). These imply that the contact point c is not known a priori but has to be determined as well (“moving boundary problem”).

In the next section we will show how one can set up the appropriate mathematical formulation of the problem to get membrane profiles and force-indentation curves.

III. SHAPE EQUATION AND APPROPRIATE BOUNDARY CONDITIONS

To describe the shape of the membrane we use two different kinds of parametrization (see Fig. 1): for the linear approximations it is sufficient to use “Monge” gauge

where the position of the membrane is given by a height $h(\rho)$ above (or below) the underlying reference plane. The disadvantage of this parametrization is that it does not allow for “overhangs”. These may be present in the full nonlinear problem; we will thus use the “angle-arc length” parametrization in the exact calculations: the angle $\psi(s)$ with respect to the horizontal substrate as a function of arclength s fully describes the shape.

A. Linear approximations

To get the profile of the free membrane one has to solve the appropriate Euler-Langrange (“shape”) equation. This equation is typically a fourth order nonlinear partial differential equation and thus in most cases impossible to solve analytically. One may, however, consider cases where the membrane is indented only a little and gradients are small. In that case one may linearize the energy functional. In the constant indentation ensemble one gets for the free part

$$E = \int_{\Sigma_{\text{free}}} dA_{\parallel} \left[\frac{\kappa}{2} (\nabla^2 h) + \frac{\sigma}{2} (\nabla h)^2 \right], \quad (4)$$

where dA_{\parallel} is the area element of the reference plane and Σ_{free} is the projected surface of the free pore-spanning membrane. The symbol ∇ denotes the two-dimensional gradient operator in the reference plane.

The appropriate shape equation can be derived by setting the first variation of energy (4) to zero, yielding

$$\nabla^2 (\nabla^2 - \frac{1}{\lambda^2}) h = 0. \quad (5)$$

The solution to this equation is a linear combination of the eigenfunctions of the Laplacian corresponding to the eigenvalues 0 and λ^{-2} . For axial symmetry it is given by $h(\rho) = h_1 + h_2 \ln(\rho/\lambda) + h_3 I_0(\rho/\lambda) + h_4 K_0(\rho/\lambda)$, where I_0 and K_0 are the modified Bessel functions of the first and the second kind, respectively [29]. The constants h_1, \dots, h_4 are determined from the appropriate boundary conditions (see Appendix A):

$$h(R_{\text{pore}}) = 0, \quad h(c) = -h_0 + \frac{c^2}{2R_{\text{tip}}}, \quad (6a)$$

$$h'(R_{\text{pore}}) = 0, \quad h'(c) = \frac{c}{R_{\text{tip}}}, \quad (6b)$$

$$\text{and} \quad h''(c) = \frac{1}{R_{\text{tip}}} - \sqrt{\frac{2w}{\kappa}}, \quad (6c)$$

where the dash denotes derivatives with respect to ρ . Five boundary conditions are needed here because neither the contact point c nor the four constants h_1, \dots, h_4 are known a priori.

The solution of the boundary value problem (5,6) can be used in two ways to calculate the force for a prescribed indentation: first, one can insert the profile back into the energy, which will then parametrically depend on the

indentation h_0 . A derivative of the energy with respect to h_0 yields the force F . Second, one can also consider stresses: in analogy to elasticity theory [30] F is given by the integral of the flux of stress through a closed contour around the tip.

The second approach is used in the present work; it has the advantage that the final expression for the force can be written in a closed form [7] (see also Appendix B):

$$F = 2\pi R_{\text{pore}} \times \kappa \frac{\partial K}{\partial \rho} \Big|_{\rho=R_{\text{pore}}}. \quad (7)$$

B. Complete nonlinear formulation

Let us now shift to the angle-arc length parametrization and consider the full nonlinear problem. In principle, the constant height ensemble could be used here as well. It is, however, much easier to fix F instead in order to fulfill the boundary conditions at the rim of the pore (see below and Appendix C).

In this paragraph all variables with a tilde are scaled with $\pi\kappa$, *i.e.* : $\tilde{E} := E/(\pi\kappa)$, $\tilde{F} := F/(\pi\kappa)$, etc. The energy functional of the free membrane can then be written as [10, 11, 12, 13]:

$$\tilde{E} = \int_{\underline{s}}^{\bar{s}} ds \tilde{L} = \int_{\underline{s}}^{\bar{s}} ds \left\{ \rho \left(\dot{\psi} + \frac{\sin \psi}{\rho} \right)^2 + \frac{2\rho}{\lambda^2} + \lambda_{\rho} (\dot{\rho} - \cos \psi) - \tilde{F} \sin \psi \right\}, \quad (8)$$

where \underline{s} is the arclength at the contact point c and \bar{s} the arclength at R_{pore} . The dot denotes the derivative with respect to s . The Langrange multiplier function λ_{ρ} helps to connect ψ and ρ to ensure that the geometric condition $\dot{\rho} = \cos \psi$ is fulfilled everywhere.

In order to make the numerical integration easier let us rewrite the problem in a Hamiltonian formulation [10, 11, 13]. The conjugate momenta are $p_{\psi} = \frac{\partial \tilde{L}}{\partial \dot{\psi}} = 2\rho \left(\dot{\psi} + \frac{\sin \psi}{\rho} \right)$ and $p_{\rho} = \frac{\partial \tilde{L}}{\partial \dot{\rho}} = \lambda_{\rho}$. The (scaled) Hamiltonian is then given by

$$\begin{aligned} \tilde{H} &= \dot{\psi} p_{\psi} + \dot{\rho} p_{\rho} - \tilde{L} \\ &= \frac{p_{\psi}^2}{4\rho} - \frac{p_{\psi} \sin \psi}{\rho} - \frac{2\rho}{\lambda^2} + p_{\rho} \cos \psi + \tilde{F} \sin \psi. \end{aligned} \quad (9)$$

Note that \tilde{H} is not explicitly dependent on s and is thus a conserved quantity. Instead of one fourth order one then has four first order ordinary differential equations,

the Hamilton equations:

$$\dot{\psi} = \frac{\partial \tilde{H}}{\partial p_\psi} = \frac{p_\psi}{2\rho} - \frac{\sin \psi}{\rho} \quad (10a)$$

$$\dot{\rho} = \frac{\partial \tilde{H}}{\partial p_\rho} = \cos \psi \quad (10b)$$

$$\dot{p}_\psi = -\frac{\partial \tilde{H}}{\partial \psi} = \left(\frac{p_\psi}{\rho} - \tilde{F} \right) \cos \psi + p_\rho \sin \psi \quad (10c)$$

$$\dot{p}_\rho = -\frac{\partial \tilde{H}}{\partial \rho} = \frac{p_\psi}{\rho} \left(\frac{p_\psi}{4\rho} - \frac{\sin \psi}{\rho} \right) + \frac{2}{\lambda^2}. \quad (10d)$$

These equations can be solved numerically with the following boundary conditions (see also Appendices A and C):

$$\psi(\bar{s}) = 0, \quad \psi(\underline{s}) = \alpha, \quad (11a)$$

$$\dot{\psi}(\underline{s}) = \frac{(\cos \alpha)^3}{R_{\text{tip}}} - \sqrt{\frac{2w}{\kappa}}, \quad (11b)$$

$$\text{and } \tilde{H} = 0, \quad (11c)$$

where contact point c and contact angle α are connected via $c = R_{\text{tip}} \tan \alpha$. The solution to (10,11) gives the indentation h_0 for some prescribed force \tilde{F} .

IV. RESULTS

This chapter will summarize the characteristic features of the solution to the boundary value problems (5,6) and (10,11).

We will scale further variables to make generalizations of the results easier: lengths will be scaled with R_{tip} . We also define

$$\tilde{\sigma} := \frac{\sigma R_{\text{tip}}^2}{\kappa}, \quad \tilde{w} := \frac{2wR_{\text{tip}}^2}{\kappa} \quad \text{and} \quad \tilde{f} := \frac{FR_{\text{tip}}}{\pi\kappa}. \quad (12)$$

In a typical experiment the curvature of the tip is of the order of ten nanometer (5–40 nm) and pore radii may lie between 30 and 200 nm [31]. The bending rigidity of a fluid membrane may vary between one and a hundred $k_B T$ [32]. One expects a maximum surface tension of the order of a few mN/m which is approximately the rupture tension for a fluid phospholipid bilayer [33]. A maximum value of the adhesion can be found by assuming that a few $k_B T$ per lipid is stored if membrane and tip are in contact. One arrives at approximately $w_{\text{max}} = 0.01 \text{ J/m}^2$. For the continuum theory to be valid Eqns. (6c,11b) imply that $\sqrt{2w/\kappa}$ is lower or equal to $1/d$, where $d \approx 5 \text{ nm}$ is the thickness of the membrane. This estimate yields approx. the same value for w_{max} as before if $\kappa = 100 \text{ k}_B T$.

Thus, $\tilde{\sigma}$ and \tilde{w} can in principle vary between 0 and 10^3 . Realistically, if we set $R_{\text{tip}} = 10 \text{ nm}$ and consider a typical fluid phospholipid bilayer (where $\kappa \approx 20 \text{ k}_B T$ [32]), $\tilde{\sigma}$ and \tilde{w} are of the order of 1. Furthermore, we will focus on a pore radius of $\tilde{R}_{\text{pore}} = 3$ in the following.

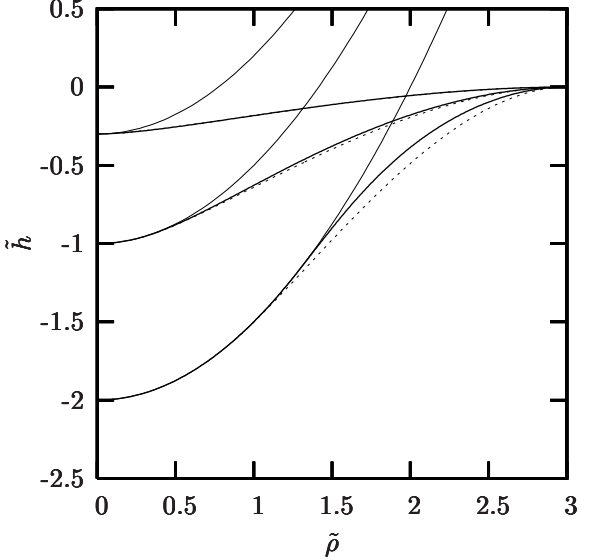


FIG. 2: Membrane profiles for different indentations \tilde{h}_0 , all for $\tilde{\sigma} = 1$ (solid lines: nonlinear calculations, dashed lines: linear approximation). The corresponding forces $\tilde{f}(\tilde{h}_0)$ for the three different indentations are (nonlinear calculations): $\tilde{f}(0.3) = 0.81$, $\tilde{f}(1) = 2.45$, $\tilde{f}(2) = 4.27$.

Let us first consider the case where there is no adhesion between tip and membrane ($\tilde{w} = 0$).

A. No adhesion between tip and membrane

In Fig. 2 the shapes of the membrane for different values of indentation are presented in scaled units. The linear calculations are dotted whereas the exact result is plotted with solid lines. For small indentations the two solutions overlap; for increasing \tilde{h}_0 , however, the deviations become larger just as one expects for a small gradient approximation (see also Ref. [15] for another example). It is clear that these differences also cause different values of the force for a fixed indentation depending on whether one calculates the approximate or the exact shape.

A deeper indentation also means that the tip has to exert a higher force. In Figs. 3 and 4 log-log plots of force-distance curves for different values of $\tilde{\sigma}$ are shown. The dashed line marks the maximum indentation $\tilde{h}_{0,\text{max}} = \tilde{R}_{\text{pore}}^2/2$ which is allowed by the geometry of tip and pore. In the limit of high forces \tilde{f} all curves converge and approach $\tilde{h}_{0,\text{max}}$; for small forces the curves are linear in \tilde{f} .

The smaller $\tilde{\sigma}$, the less force has to be applied to reach the same indentation (see Fig. 3). For decreasing $\tilde{\sigma}$ the force-distance curves converge to the curve where $\tilde{\sigma} = 0$, which is plotted dashed-dotted in Fig. 3. In the other limit ($\tilde{\sigma} \rightarrow \infty$) the curves become essentially linear in $\tilde{\sigma}$ as can be seen clearly after scaling out the tension (see

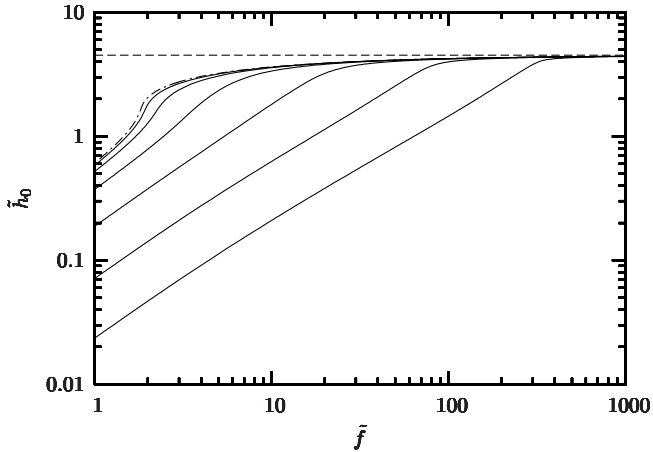


FIG. 3: Force-distance curves for $\tilde{w} = 0$ and $\tilde{\sigma} = \frac{1}{16}, \frac{1}{4}, 1, 4, 16$ and 64 (σ increasing from left to right). The curve for $\tilde{\sigma} = 0$ is dashed-dotted.

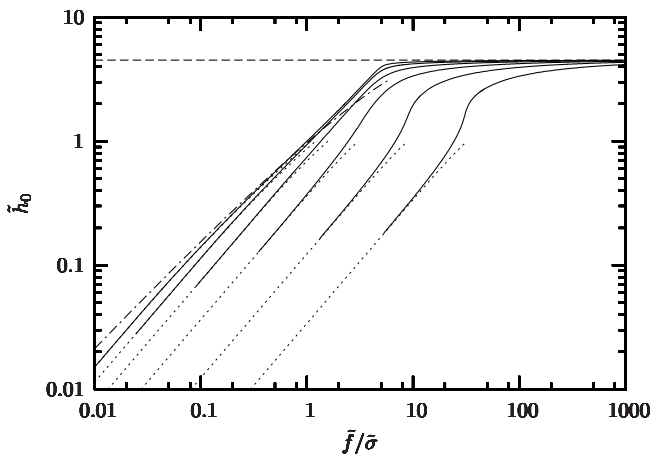


FIG. 4: Scaled force-distance curves for $\tilde{w} = 0$ and $\tilde{\sigma} = \frac{1}{16}, \frac{1}{4}, 1, 4, 16$ and 64 (σ increasing from right to left). The solution for $\tilde{\sigma} \rightarrow \infty$ in the linear regime is dashed-dotted. Nonlinear results are plotted with solid lines, the linear approximation is dotted.

Fig. 4). It is possible to calculate the limiting curve in the linear regime: for $\tilde{\sigma} \rightarrow \infty$ (*i.e.* $\kappa \rightarrow 0$) the linearized Euler Lagrange equation is simply the Laplace equation, $\Delta h = 0$, which is solved by $h(\rho) = d_1 + d_2 \ln \frac{\rho}{R_{\text{pore}}}$ in the present symmetry. The constants d_1 and d_2 can be determined with the help of the two boundary conditions $h(R_{\text{pore}}) = 0$ and $h(c) = -h_0 + \frac{c^2}{2R_{\text{tip}}}$. The contact point c is then determined by an energy minimization. The final result for the indentation depth is:

$$\tilde{h}_0^{\tilde{\sigma} \rightarrow \infty} = \frac{\tilde{f}/\tilde{\sigma}}{4} \left[1 - \ln \left(\frac{\tilde{f}/\tilde{\sigma}}{2\tilde{R}_{\text{pore}}^2} \right) \right], \quad (13)$$

which is plotted dashed-dotted in Fig. 4. At any given penetration the force is now strictly proportional to the

tension. Notice also the remarkably weak (logarithmic) dependency of penetration on pore size.

B. Including adhesion between tip and membrane

In this section we will also allow for adhesion between tip and membrane, *i.e.* \tilde{w} is not necessarily equal to zero. This will change the qualitative behavior of the force-distance curves dramatically: for fixed $\tilde{\sigma}$ and \tilde{w} different branches can be found in the force-distance curve. A hysteresis may occur as well as we will see in this section. Additionally, stable membrane profiles exist even if the tip is pulled upwards. It is therefore possible to calculate the maximum pulling force that can be applied before the tip detaches from the membrane and relate it to the value of the adhesion between tip and membrane.

In Fig. 5 membrane profiles for an adhesion of $\tilde{w} = 2$ and different values of \tilde{f} are plotted. The scaled surface tension $\tilde{\sigma}$ is fixed to 1. Depending on the chosen parameter values one can sometimes find more than one profile that solves the underlying boundary value problem (see also below). In Fig. 5 an example is given for a force of $\tilde{f} = 0.5$ where three profiles can be found (see dashed curves in Fig. 5). The thin dashed solutions are the ones that are higher in energy compared to the thicker profile. If the scaled force \tilde{f} was fixed to 0.5 in an experiment, one thus would expect the thick dashed profile to occur. We will, however, see in the following that the upper thin dashed profile is metastable and thus also a possible state the system can find in.

A profile can also exhibit “overhangs”: with this notion we denote parts of the free shape where the absolute value of the angle $\psi(s)$ exceeds 90 degrees (see Fig. 1).

If we at first omit solutions that exhibit such overhangs, we arrive at force-distance curves like the ones plotted in Fig. 6 for $\tilde{\sigma} = 1$ and changing \tilde{w} . Compared to the case without adhesion, where a distinct linear behavior was found for small forces, we now also observe “S-shaped” functions. Every point on the curves corresponds to a profile where the contact curvature condition (6c,11b) is fulfilled. This implies that the energy of the free membrane has a *local extremum* at the corresponding contact angle if plotted as a function of $\alpha \in [0, \pi/2)$ [15]. Here one finds that those parts of the force-distance curve that have a negative slope are maximum points in the energy (*i.e.* unstable equilibrium profiles) whereas those with a positive slope are (meta)stable minima.

In the inset of Fig. 6 the region of instability for the curve with $\tilde{w} = 2$ is plotted. The dotted line corresponds to local maxima, the dashed parts of the curve are local minima. Those points of the curve where the energy of the corresponding profile is a *global minimum* are connected with a solid line. At $\tilde{f} = 0.414$, this line exhibits a jump: the two minima in the corresponding indentation-energy plot have the same value there (28.2κ). Because an energy barrier of about 1κ has to be crossed to get

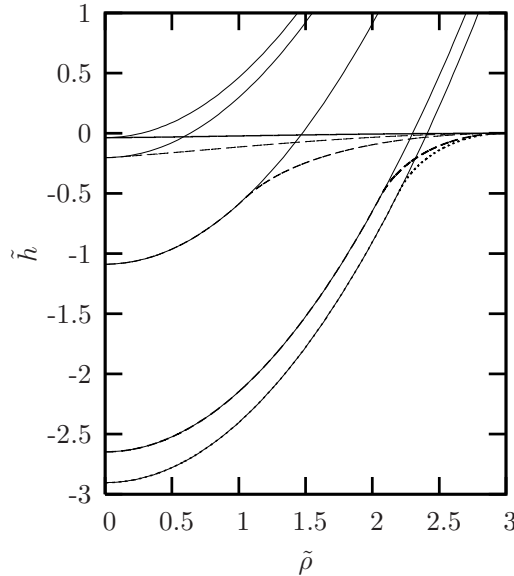


FIG. 5: Membrane profiles for an adhesion of $\tilde{w} = 2$ and different forces $\tilde{f} = 0.1$ (solid), 0.5 (long dashes) and 1.0 (dotted). The scaled surface tension $\tilde{\sigma}$ is fixed to 1 . Note that one finds three profiles for $\tilde{f} = 0.5$ where the thinner curves are the ones with higher energy. The corresponding indentations $\tilde{h}_0(\tilde{f})$ for the three different forces are (nonlinear calculations): $\tilde{h}_0(0.1) = 0.04$, $\tilde{h}_0^i(0.5) = 0.20$, $\tilde{h}_0^{ii}(0.5) = 1.09$, $\tilde{h}_0^{iii}(0.5) = 2.65$, and $\tilde{h}_0(1.0) = 2.90$.

from one indentation to the other one, thermal fluctuations cannot cause a transition between the two states if we consider a typical fluid phospholipid bilayer where κ is of the order of many $k_B T$. This gives rise to a hysteresis depending on the starting point of an experiment (increasing force starting from zero vs. decreasing starting from high forces). If the force is increased starting from zero in the experiment, one observes a snap-on of the AFM-tip as soon as the barrier is crossed. Notice that at that moment the tip is already in contact with the membrane, in contrast to what one would naively expect. The amount of indentation before the snap-on is, however, rather small compared to the snap-on itself.

The open circles plotted in the inset of Fig. 6 correspond to the profiles shown in Fig. 5. With the help of the discussion in the last paragraph one can assign the three profiles of $\tilde{f} = 0.5$ to different extrema: the two unstable solutions (thin dashed lines) are the local minimum and maximum, respectively, whereas the stable solution (thick dashed line) is the global minimum. The energy barrier to get from the local to the global minimum is already a bit lower (approx. 0.5κ) than the one of the jump point where $\tilde{f} = 0.414$. For a fluid phospholipid bilayer this is, however, still reasonably high compared to the thermal energy which is why one may also find the system in the metastable local minimum at $\tilde{f} = 0.5$ in an experiment.

For \tilde{w} higher than a certain threshold \tilde{w}_0 the tip is

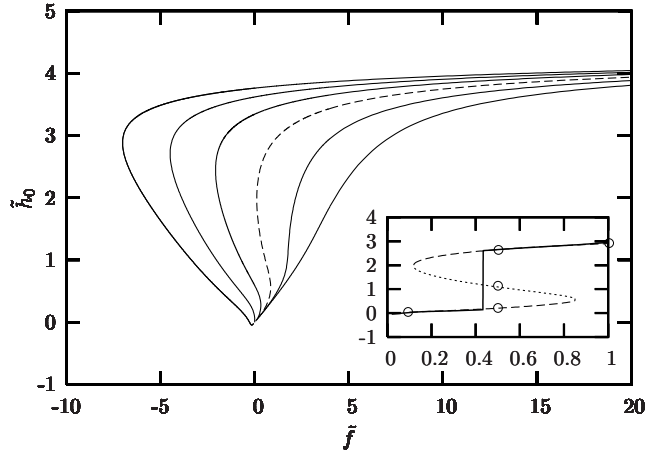


FIG. 6: Force-distance curves for $\tilde{\sigma} = 1$ and $\tilde{w} = 0, 1, 2, 3, 4, 5$ (from right to left). The curve for $\tilde{w} = 2$ for small values of \tilde{f} is plotted in the inset. In this case the energy barrier at $\tilde{f} = 0.414$ is approx. 1κ . The profiles for the points marked with open circles (\circ) can be found in Fig. 5. Note that a second branch (the one consisting of profiles with overhangs) is omitted here (cf. Fig. 7).

already sucked into the pore if there is no force at all. One can then obtain stable solutions even when pulling upwards (where $\tilde{f} < 0$) [34]. This also implies that, for $\tilde{w} = \tilde{w}_0$, an infinitesimal pulling force will suffice to unbind tip and membrane, even though the adhesion between tip and membrane is greater than zero. It is important to keep that fact in mind if one wants to interpret measurements of AFM experiments such as the one described here.

If we now allow for overhangs and consider higher values of \tilde{w} (or lower values of $\tilde{\sigma}$), the force-indentation curves show an even richer behavior: a second branch can be found which is higher in energy than the one already discussed. Fig. 7 shows one example where $\tilde{\sigma} = 1$ and \tilde{w} is varied between 0 and 20 .

Again, points of the plotted curves correspond to profiles that are local extrema of the energy as a function of α . New is, however, that one can find cases where the energy is not differentiable any more for certain values of α . Points where this is the case can nevertheless be local extrema and have to be respected in a stability analysis although conditions (6c,11b) are not fulfilled there any more. We will not go thoroughly into detail with that in this work but will come back to that point at the end of this section.

Let us at first consider how the new branch (omitted in Fig. 6) evolves for increasing \tilde{w} : for $\tilde{w} = 0$ and 5 it consists completely of indented profiles which exhibit overhangs. These are equilibrium solutions with energies higher than those of the already known part of the curve from Fig. 6. One example of a typical profile ($\tilde{w} = 5, \tilde{f} = 10$) is depicted in inset e of Fig. 7. In principle, one can find further solutions of the shape equations by allowing

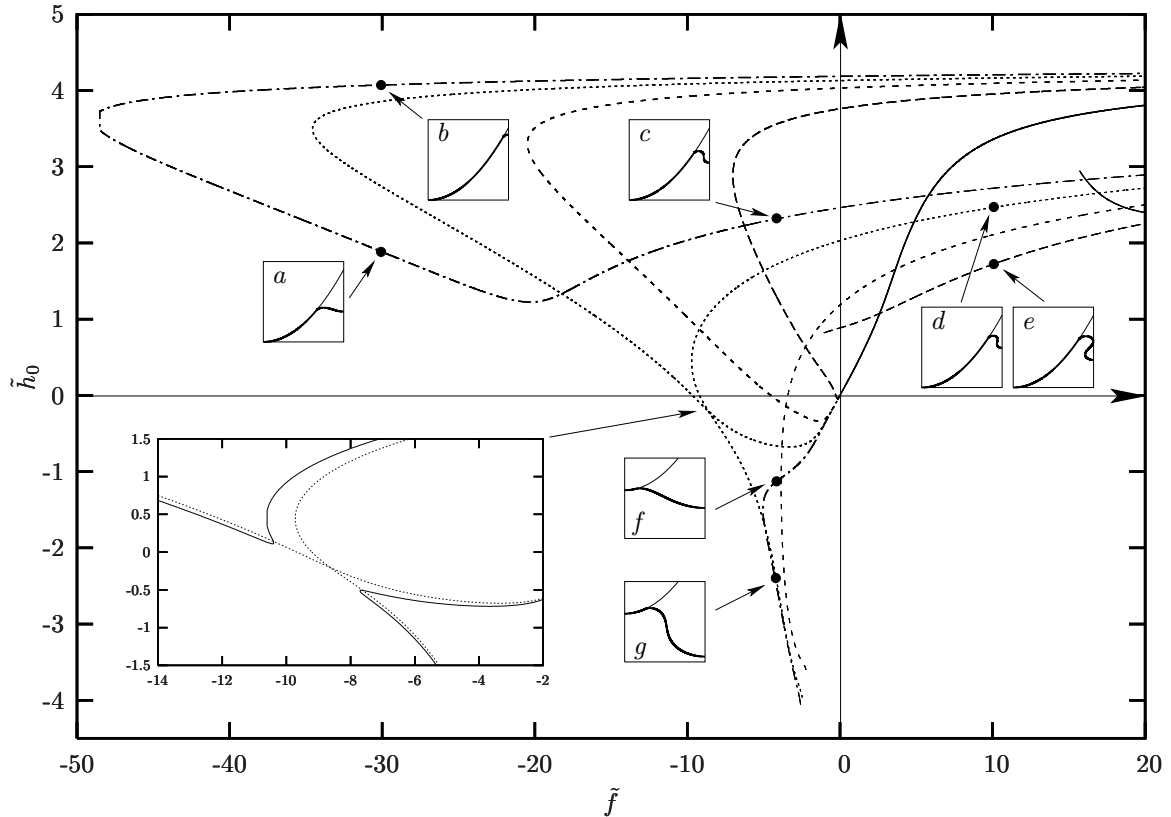


FIG. 7: Force-distance curves for $\tilde{\sigma} = 1$ and $\tilde{w} = 0$ (solid), 5 (long dashes), 10 (short dashes), 15 (dotted) and 20 (dashed-dotted). A thinner line style is used for those parts of the curves where the corresponding profiles exhibit overhangs. In the insets a - g profiles for different values of (\tilde{f}, \tilde{h}_0) are depicted (scaling is $\tilde{h} : \tilde{\rho} = 5 : 3$). In the inset on the left lower corner the “branch splitting” is shown as discussed in the text ($\tilde{w} = 15.0$ (dotted line) and 15.5 (solid line)).

profiles with two or more overhangs. These are, however, not shown here because their energies are still higher than the ones of the “one overhang” branch.

If we increase \tilde{w} to 10, we find an overhang branch as well, but now also profiles with a *negative* h_0 exist. Consequently, new and old branch intersect each other.

In the case of $\tilde{w} = 15$ and 20 the new branch consists of both overhang and non-overhang profiles. This should not surprise us too much as the difference between a profile with or without an overhang is not a structural one but was just introduced artificially in our terminology. A typical profile of the new branch for $\tilde{w} = 15$ and positive force is plotted in inset d of Fig. 7. Note that its shape is analogous to that of profile e where \tilde{w} was equal to 5.

Between $\tilde{w} = 15$ and 15.5 the two branches, that intersected for slightly lower values, suddenly split into two separate branches if \tilde{w} is increased (see inset in the lower left corner of Fig. 7). For higher adhesion, the *new* branch is connected to the origin instead of the original one.

As mentioned, all new branches described in the last paragraphs are higher in energy than those originally discussed. The *global* energy minima for $\tilde{w} \neq 0$ in the constant force ensemble can be found at those parts of the

curve where the indentation is already quite high. To give an impression what typical profiles look like insets a and b show an example for global maximum and global minimum, respectively, for $\tilde{f} = -30$ and $\tilde{w} = 20$.

A possible measurable quantity in the experiment is the detachment force which is the maximum pulling force \tilde{f}_{det} where the tip is close to detachment but still in contact with the membrane. In Fig. 8 this detachment force is plotted as a function of \tilde{w} for different values of $\tilde{\sigma}$. Starting from a certain threshold adhesion $\tilde{w}_{\text{thr}}(\tilde{\sigma})$ the detachment force decreases with increasing \tilde{w} and exhibits a linear behavior for higher adhesions. Increasing $\tilde{\sigma}$ also increases the threshold adhesion (e.g. $\tilde{w}_{\text{thr}}(\frac{1}{16}) = 0.22$ compared to $\tilde{w}_{\text{thr}}(1) = 1.25$). At higher values of $\tilde{\sigma}$ other qualitative features (such as additional instabilities) occur. However, these ramifications will not be discussed in the present work.

Characteristically, the detachment happens at deep indentations (\tilde{h}_0 close to the maximum indentation possible). In contrast, in the literature reports on bilayers being pulled out in the opposite direction (so-called “tethers”) can be found [13, 16, 18]. In our calculations we indeed find profiles that exhibit a similar behavior but these solutions are energetically unstable: for a given force

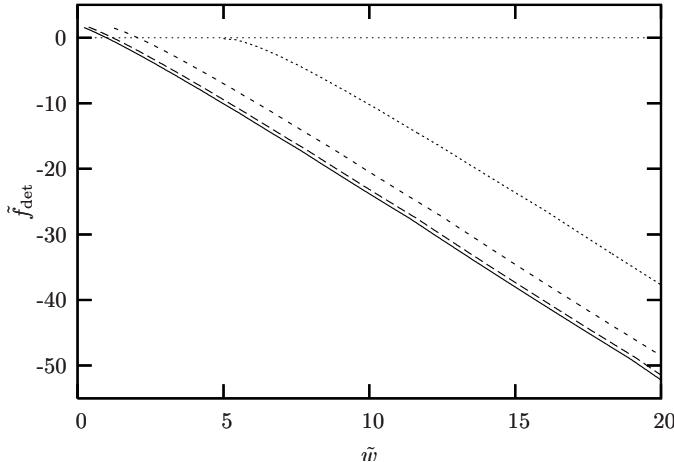


FIG. 8: Detachment force as a function of adhesion for $\tilde{\sigma} = \frac{1}{16}, \frac{1}{4}, 1$ and 4 ($\tilde{\sigma}$ increasing from left to right).

they are always higher in energy than the corresponding deep-indented solution of the shape equation. This is due to the adhesion balance we choose: it is more favourable for the tip to be sucked in completely and gain adhesion energy instead of pulling a tether. Consider, for instance, the case where $\tilde{w} = 20$ and $\tilde{f} = -4$. In the insets *c*, *f* and *g* of Fig. 7 the corresponding profiles are plotted: the global energy minimum can be found at higher indentations and resembles profile *b*. Profile *c* is a local minimum which is still lower in energy than profiles *f* and *g*. The latter are local maxima and thus unstable tether-states. In-between one can find a local minimum that does not fulfill the contact boundary conditions (6c,11b). If one moves to slightly lower forces (*e.g.* $\tilde{w} = 20$ and $\tilde{f} = -5$), one also finds profiles that do fulfill the contact boundary conditions and are metastable local minima.

Our calculations cannot, however, explain existing experiments where tethers of micrometer size were generated [18, 35]. Consequently, the assumption of an adhesion balance does not seem to be correct there. It may, however, as well be that kinetic effects cause the system to stay in a metastable state. How one could possibly try to include an adhesion balance into the whole experimental setup will be part of the discussion in the next section.

V. DISCUSSION

In the previous sections we have discussed the indentation of a pore-spanning bilayer by an AFM tip. We found that the force-distance curves show a linear behavior for small forces if the adhesion between tip and membrane vanishes. This is in agreement with recent experiments [7].

It is important to note that the linear behavior in these existing measurements poses a problem if one wants to

make predictions about the value of the elastic material constants σ and κ : the slope of the curves is the only parameter that can be extracted from the experiment [36]. In the theory, however, σ and κ need to be known to calculate the curve. Fitting two parameters to a line is not possible. Thus, one either has to determine one of the two constants with a different measurement or one takes the adhesion w between tip and membrane into account by increasing w experimentally: as we have seen, the curves change their behavior dramatically for $w \neq 0$. It should thus be possible to fit two parameters to the resulting curves which would yield a local κ and σ in one fell swoop whereas w can simultaneously be determined from the snap-on of the tip upon approach to the bilayer. The experimentalist, however, has to make sure in that case that the line of contact between tip and membrane is really due to a force balance as described in this paper and not due to other effects such as pinning of the membrane to single spots on the tip. In practice, this is rather difficult and will be a challenge for future experiments.

Our theoretical approach does not account for hydrodynamic effects although the whole setup is in water and the AFM tip is moved with a certain velocity. First measurements have shown, however, that it is possible to increase the velocity of the tip up to $60 \mu\text{m s}^{-1}$ without altering the force-distance curves dramatically, at least if an adhesion between tip and membrane is small enough [7]. Complications arising from a correct hydrodynamical treatment were thus omitted here.

Including adhesion, the velocity of the measurement should nevertheless be as slow as possible to ensure that the line of contact equilibrates due to the force balance. If this is guaranteed, one can also check whether the predicted linear behavior between detachment force and adhesion is actually valid. This may be subject of future work.

Acknowledgments

We thank Siegfried Steltenkamp, Andreas Janshoff, and Jemal Guven for helpful discussions. MD acknowledges financial support by the German Science Foundation through grant De775/1-3.

APPENDIX A: BOUNDARY CONDITIONS

In this appendix we will explain the origin of the boundary conditions (6) and (11): Eqns. (6a) follow simply from the requirement of continuity at the pore rim and the point where the membrane leaves the tip. Asking for a membrane that has no kinks and thus no diverging bending energy gives Eqns. (6b) and (11a).

If the membrane is free to choose its point of detachment as it is assumed here, an adhesion balance at the tip yields another boundary condition for the contact curvatures (6c/11b) [19, 20]. In Ref. [15] a quick derivation

can be found for the axisymmetric case in the constant height ensemble: varying the point of contact changes the energy of the free profile but also the energy due to the part at the tip. By setting the total variation to zero one obtains the well-known contact curvature condition (Eqn. (6c) in Monge gauge). Observe that this assumes differentiability of the energy as a function of contact point position. In the force ensemble an extra term $\tilde{F}\delta h$ has to be added to the variation of the bound membrane. A term that is equal and opposite, however, enters the variation of the free membrane via the Hamiltonian (9). In total, both terms cancel and one again obtains the same condition (Eqn. (11b) in angle-arc length parametrization).

The remaining boundary condition (11c) can be found by considering the possible variations at the rim of the pore: the only thing that can happen is that additional membrane is pulled horizontally into the pore. Variations of radius, height or angle are not allowed. Thus, a variation of the energy comprises only the term $-\tilde{H}\delta s$. Setting this to zero gives $\tilde{H}(\bar{s}) = 0$ at the rim [11]. The Hamiltonian is, however, a constant with respect to s . Thus, it is equal to zero everywhere along the free membrane.

APPENDIX B: CALCULATION OF THE FORCE VIA THE STRESS TENSOR

If the shape of the free membrane is known, the stress tensor \mathbf{f}^a ($a \in \{1, 2\}$) can be evaluated at every point of the surface Σ_{free} . The integral of its flux through an arbitrary contour γ which encloses the tip gives the force [37]

$$F = \mathbf{e}_h \cdot \oint_{\gamma} ds \left\{ \left[\frac{\kappa}{2} (K_{\perp}^2 - K_{\parallel}^2) - \sigma \right] \mathbf{l} - \kappa (\nabla_{\perp} K) \mathbf{n} \right\}. \quad (\text{B1})$$

The normal vectors \mathbf{l} and \mathbf{n} are perpendicular to γ and to each other as well in every point of the curve. In addition, \mathbf{l} is tangential to the surface whereas \mathbf{n} is normal to it.

K_{\perp} and K_{\parallel} are the curvatures perpendicular (in direction of \mathbf{l}) and tangential to the curve. The symbol ∇_{\perp} denotes the derivative along \mathbf{l} .

This rather abstract formula can be translated into “Monge gauge”. If we exploit axial symmetry by integrating around a circle of radius $\rho = R_{\text{int}}$, Eqn. (B1) reads

$$F = -2\pi R_{\text{int}} \left\{ \left[\frac{\kappa}{2} \left(\frac{h''(\rho)^2}{g^3} - \frac{h'(\rho)^2}{\rho^2 g} \right) - \sigma \right] \frac{h'(\rho)}{\sqrt{g}} \right. \\ \left. + \kappa \left(\frac{h''(\rho)}{\sqrt{g}^3} + \frac{h'(\rho)}{\rho \sqrt{g}} \right)' \frac{1}{g} \right\}_{\rho=R_{\text{int}}}, \quad (\text{B2})$$

where $g = 1 + h'(\rho)^2$. Note that the dash denotes derivatives with respect to ρ .

If in particular we choose to evaluate the force at $R_{\text{int}} = R_{\text{pore}}$, the expression (B2) simplifies considerably to Eqn. (7).

APPENDIX C: NUMERICAL CALCULATIONS

The Hamilton equations (10) were solved by using a shooting method [38]: for a trial contact point c Eqns. (10) were integrated with a fourth-order Runge-Kutta method. The value of c determined the contact angle α and with it ψ , ρ , p_{ψ} , and p_{ρ} at $s = \underline{s}$ via the boundary conditions (11). The integration was stopped as soon as ρ was equal or greater than R_{pore} . To reach R_{pore} exactly one extra integration with the correct step-size backwards was performed. Finally, the value(s) of c for which $\psi = 0$ at R_{pore} were identified for fixed parameters F , σ , w , etc.

If the calculation had been done in the constant height ensemble, one would additionally have to check whether the correct indentation h_0 was reached at $\rho = R_{\text{pore}}$ after shooting. In the constant force ensemble this complication of meeting a second condition is avoided which is why we chose to use it for the nonlinear calculations.

[1] H. Lodish, A. Berk, S. L. Zipursky, P. Matsudaira, D. Baltimore, and J. Darnell, *Molecular Cell Biology* (Freeman & Company, New York, 2000).

[2] J. Dai and M. P. Sheetz, in *Laser Tweezers in Cell Biology*, edited by M. P. Sheetz (Academic Press, San Diego, 1998), and references therein.

[3] R. Kwok and E. Evans, *Biophys. J.* **35**, 637 (1981). E. Evans and D. Needham, *J. Phys. Chem.* **91**, 4219 (1987).

[4] W. Rawicz, K. C. Olbrich, T. McIntosh, D. Needham, and E. Evans, *Biophys. J.* **79**, 328 (2000).

[5] A. Alessandrini and P. Facci, *Meas. Sci. Technol.* **16**, R65 (2005).

[6] S. Sen, S. Subramanian, and D. E. Discher, *Biophys. J.* **89**, 3203 (2005);

[7] S. Steltenkamp *et al.*, submitted.

[8] S. Svetina and B. Žekš, *Eur. Biophys. J.* **17**, 101 (1989);

[9] L. Miao, B. Fourcade, M. Rao, M. Wortis, and R. K. P. Zia, *Phys. Rev. A* **43**, 6843 (1991).

[10] U. Seifert, K. Berndl, and R. Lipowsky, *Phys. Rev. A* **44**, 1182 (1991).

[11] F. Jülicher and U. Seifert, *Phys. Rev. E* **49**, 4728 (1994).

[12] U. Seifert, *Adv. Phys.* **46**, 13 (1997).

[13] A.-S. Smith, E. Sackmann, and U. Seifert, *Europhys. Lett.* **64**, 281 (2003).

[14] M. Deserno and T. Bickel, *Europhys. Lett.* **62**, 767 (2003).

[15] M. Deserno, *Phys. Rev. E* **69**, 031903 (2004).

[16] T. R. Powers, G. Huber, and R. E. Goldstein, *Phys. Rev.*

E **65**, 041901 (2002); I. Derényi, F. Jülicher, and J. Prost, Phys. Rev. Lett. **88**, 238101 (2002).

[17] A.-S. Smith, E. Sackmann, and U. Seifert, Phys. Rev. Lett. **92**, 208101 (2004).

[18] G. Koster, A. Cacciuto, I. Derényi, D. Frenkel, and M. Dogterom, Phys. Rev. Lett. **94**, 068101 (2005).

[19] L. D. Landau and E. M. Lifshitz, *Theory of Elasticity*, 3rd ed. (Butterworth-Heinemann, Oxford, 1986), Sec. 12, problem 6.

[20] U. Seifert and R. Lipowsky, Phys. Rev. A **42**, 4768 (1990).

[21] A. Boulbitch, Europhys. Lett. **59**, 910 (2002).

[22] Note that the part of the system outside the pore just acts like a reservoir fixing the lateral tension. Its energetics do not have to be considered explicitly.

[23] F. David and S. Leibler, J. Phys. II **1**, 959 (1991).

[24] P. B. Canham, J. Theoret. Biol. **26**, 61 (1970).

[25] W. Helfrich, Z. Naturforsch. **28c**, 693 (1973).

[26] M. Do Carmo, *Differential Geometry of Curves and Surfaces*, (Prentice Hall, 1976); E. Kreyszig, *Differential Geometry*, (Dover, New York, 1991).

[27] The convention used in this article is that a sphere with outward pointing normal vector has a positive K .

[28] The Gauss-Bonnet theorem states that:

$$\int_{\Sigma} dA K_G = 2\pi - \int_{\partial\Sigma} ds K_g ,$$

for a simply connected surface [26]. In our case the boundary $\partial\Sigma$ of the surface Σ is a circle of radius R_{pore} .

Its geodesic curvature K_g is equal to R_{pore}^{-1} , such that the second integral yields 2π . Thus, the integral over the Gaussian curvature K_G is zero as long as no topological changes occur.

[29] *Handbook of Mathematical Functions*, 9th ed., edited by M. Abramowitz and I. A. Stegun (Dover, New York, 1970).

[30] L. D. Landau and E. M. Lifshitz, *Theory of Elasticity*, 3rd ed. (Butterworth-Heinemann, Oxford, 1986).

[31] S. Steltenkamp, personal communication.

[32] U. Seifert and R. Lipowsky, Morphology of vesicles; in *Handbook of Biological Physics*, vol. 1A, edited by R. Lipowsky and E. Sackmann (Elsevier, Amsterdam, 1995).

[33] E. Evans, V. Heinrich, F. Ludwig, and W. Rawicz, Biophys. J. **85**, 2342 (2003).

[34] Strictly speaking *all* of these solutions are metastable with respect to detachment of the tip from the membrane.

[35] R. M. Hochmuth, N. Mohandas, and P. L. Blackshear, Jr., Biophys. J. **13**, 747 (1973); J. Dai and H. Ping Ting-Beall and M. P. Sheetz, J. Gen. Physiol. **110**, 1 (1997).

[36] The axis intercept is needed to gauge the distance between AFM tip and substrate in the experiment and can therefore not be extracted as a second parameter.

[37] R. Capovilla and J. Guven, J. Phys. A: Math. Gen. **35**, 6233 (2002).

[38] *Numerical Recipes in C*, 2nd ed., edited by W.H. Press *et al.* (Cambridge University Press, Cambridge, 1992)